Etching Growth under Surface Confinement: An Effective Strategy To Prepare Mesocrystalline Pd Nanocorolla

Xiaoqing Huang, Shaoheng Tang, Jing Yang, Yueming Tan, and Nanfeng Zheng*

State Key Laboratory for Physical Chemistry of Solid Surfaces and Department of Chemistry, College of Chemistry and Chemical Engineering, Xiamen University, Xiamen 361005, China

S *Supporting Information*

ABSTRACT: An etching growth strategy was developed to prepare corolla-like Pd mesocrystals consisting of unidirectionally aligned, well-spaced, and connected ultrathin (1.8-nm-thick) Pd nanosheets. The combined use of CO and Fe^{3+} is critical to the successful synthesis of the branched corolla-like Pd mesocrystals. While CO functions as the surface-confining agent to allow anisotropic growth of the 1.8-nm-thick Pd nanosheets as branches, Fe^{3+} etches the Pd seeds at the early stage of the reaction to induce formation of the branched structure. Inheriting the unique properties of 1.8-nm-thick Pd nanosheets, the as-prepared Pd mesocrystals display well-defined surface plasmon resonance absorption in the near-infrared region, a high electrochemically active surface area, and a significant photothermal effect when irradiated with a near-infrared laser. Owing to the presence of internal voids and increased apparent thickness, the Pd mesocrystals also exhibit several features superior to those of single-domain Pd nanosheets, making them promising for electrocatalysis and cancer photothermal therapy applications.

Mesocrystals, single-crystal-like inorganic superstructures made of highly aligned crystalline subunits, represent an emerging new class of colloidal crystals that have unique catalytic, magnetic, electronic, and optical properties.[1−5] These highly ordered superstructures serve as structural bridges between nanoscale matter and macroscale materials.[1,2] With the efforts of a large number of research groups, mesocrystals have been prepared in a wide range of compositions, such as $CaCO_3$,[6−8] $BaCO_3$,[9] ZnO,[5,10] TiO_2,[11−13] V_2O_5,[14] NiO,[15] $Ca_3(PO_4)_2$,[16] and $CaMoO_4$.[17] To date, most of the reported mesocrystals are oxides or carbonates. Reports on the synthesis of metallic mesocrystals are rare.[18,19] However, owing to the presence of internal voids and therefore high internal surface area, metallic mesocrystals are expected to have some unique properties or advantages that cannot be possessed by single-domain metallic nanocrystals. In recent years, nanostructures of palladium, a key catalytic element, have attracted considerable interest among researchers. Various Pd nanostructures with well-defined morphologies, such as cubes,[20] polyhedra,[21,22] concave polyhedra,[23] plates,[24,25] rods/wires,[26,27] and branched nanocrystals,[27] have been successfully prepared. However, it remains a great challenge to find a method to fabricate mesocrystalline Pd nanostructures.

We now report here an etching growth strategy to prepare corolla-like Pd mesocrystals (CPdMs) consisting of connected ultrathin (1.8-nm-thick) Pd nanosheets. In the synthesis of CPdMs, CO was applied as the surface-confining agent to ensure the growth of ultrathin sheet-like branches having (111) as the main exposed surface, and a trace amount of Fe^{3+} was used to etch the Pd seeds and induce the formation of branched structure. The as-prepared Pd mesocrystals nicely inherit the unique properties of 1.8-nm-thick Pd nanosheets: (1) a well-defined surface plasmon resonance (SPR) absorption feature in the near-infrared (NIR) region, (2) a high electrochemically active surface area (EASA) ($67\ m^2/g$), and (3) a significant photothermal effect in response to a NIR laser.[24] More importantly, CPdMs offer the following three advantages over single-domain 1.8-nm-thick Pd nanosheets with a similar dynamic size in solution: (1) mass transfer in electrodes made of CPdMs is significantly enhanced by the branched structure, (2) CPdMs are more easily taken up by cancer cells, resulting in much-enhanced NIR photothermal therapy efficacy, and (3) CPdMs are more easily separated from solution by centrifugation owing to their increased apparent thickness.

To prepare CPdMs, $Pd(acac)_2$, poly(vinylpyrrolidone), and a small amount of $FeCl_3$ were mixed together with benzyl alcohol (see Supporting Information for details). The resulting homogeneous solution was transferred to a glass pressure vessel. After being charged with CO to 1 bar, the vessel was heated from room temperature to 100 °C in 30 min and kept at this temperature for 1.5 h with stirring. As the reaction progressed, the mixture experienced a significant color change from yellow to light blue, and finally deep blue. The resulting blue colloidal products were collected by centrifugation and washed several times with ethanol and acetone. The production yield of CPdMs was ∼90%, which was measured by inductively coupled plasma spectrometry (ICP).

Representative electron microscopy images of the as-made CPdMs are illustrated in Figure 1. The images show that all particles surveyed were corolla-like with multibranched subunits, demonstrating high-quality production of CPdMs. The size of CPdMs ranged narrowly from 170 to 200 nm, with an average diameter of 185 nm (Figure S1). The number of branches on each CPdM ranged up to 30, with an average of 22. The corollar feature of CPdMs was further confirmed by high angle annular dark field-scanning transmission electron microscopy (HAADF-STEM) analysis (Figures 1c, S2). Both selected area electron diffraction (SAED) and high-resolution transmission electron microscopy (HRTEM) measurements (Figure 1d,e) on individual CPdMs indicated the single-crystalline nature of these
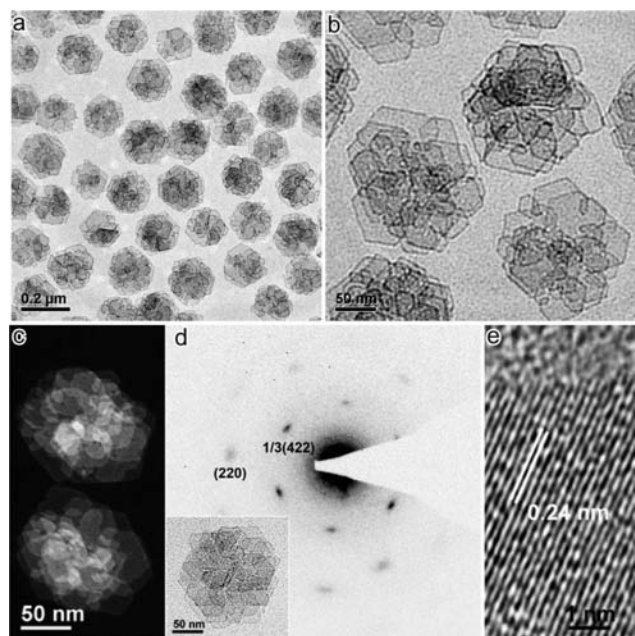
Figure 1. (a) Representative low-magnification TEM, (b) high-magnification TEM, and (c) HAADF-STEM images of as-prepared CPdMs. (d) SAED pattern of a single CPdM. Bottom-left inset shows the corresponding TEM image. (e) HRTEM image on a branch/corolla of the CPdM.
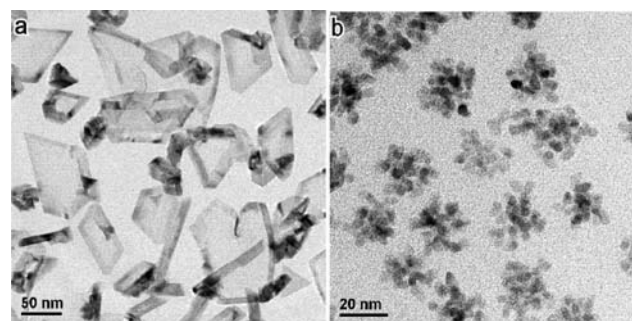

Figure 2. TEM images of Pd nanocrystals prepared under reaction conditions similar to those in Figure 1, except that the reactions were conducted in the absence of $FeCl_3$ (a) and in the absence of CO (b).

highly branched Pd nanostructures. The SAED pattern showed a series of diffraction spots with six-fold rotational symmetry. The HRTEM image showed lattice fringes with interplanar spacing of 0.24 nm, corresponding to $1/3(422)$ fringes of face-centered cubic (fcc) Pd (Figure 1e). The fcc structure of the Pd nanosheets is supported by their X-ray diffraction pattern (Figure S3). The observation of fcc Pd $1/3(422)$ fringes indicated that the palladium nanosheet branches have (111) as basal planes.[24,28,29] As verified by electrochemical CO stripping experiments in H_2SO_4, the exposed surface of the as-prepared CPdMs was indeed dominated by (111) (Figure S4).

Because of their 2D structure, CPdMs tend to lie flat on the TEM grids, making it difficult to directly analyze their side structure. By mixing CPdMs with carbon nanotubes, fortunately, some CPdMs can attach on the carbon nanotubes, enabling us to obtain the side structure of CPdMs. As clearly illustrated in the TEM image (Figure S5), the side of each CPdM consists of parallel-aligned Pd nanosheets with uniform thickness, narrowly distributed at 1.8 nm. As a whole, the thickness of each CPdM was measured to be more than 10 nm. Based on our previous work, CO binds strongly on the Pd (111) surface and therefore confines the growth of the Pd nanostructures to maximize (111) surface exposure.[24] CO is thus considered essential to the anisotropic growth of sheet-like morphology of each branch of CPdMs. In the presence of CO but the absence of $FeCl_3$, the obtained sheet-like Pd nanostructures did not have the branched feature (Figure 2a), nor was branched structure obtained when $FeCl_3$ was replaced by CTAC or $ZnCl_2$ (Figure S6). Thus, it is reasonable to propose that the presence of Fe^{3+} is the main cause of forming the branched structure in CPdMs. To support such a proposal, a reaction was carried out with Fe^{3+} but without CO. As a result, uniform dendritic Pd nanostructures with non-sheet-like branches were formed (Figures 2b, S7, S8), again confirming

the importance of CO in forming sheet-like structure in CPdMs. It should be noted that, in the literature, branched Pd nanocrystals were also prepared when Cu^{2+} was incorporated in the synthesis.[27]

While the reaction with CO but without $FeCl_3$ gave a blue colloidal solution within 20 min, the reaction mixture containing $FeCl_3$ remained yellow, and no separable particles were obtained from the reaction until 20 min. This phenomenon indicates that $FeCl_3$ greatly retarded the reduction of $Pd(acac)_2$. It is believed that the retarded reduction is due to the oxidative etching effect induced by Fe^{3+}, which has been previously demonstrated[25,30] and can be explained by the higher redox potential of Fe^{3+}/Fe^{2+} than $Pd(acac)_2/Pd, acac^-$.[31] While CO facilitates the growth of uniform Pd nanosheets, Fe^{3+} etches the Pd nanosheets that are formed. In our synthesis, CO was supplied continuously, but only a limited amount of $FeCl_3$ was supplied. As the reaction proceeded, Fe^{3+} species were continuously consumed. Once Fe^{3+} was depleted, Pd nanostructures were expected to grow to form separable CPdMs. Indeed, after 20-min reaction time, the reaction mixtures started to become blue, implying that a dramatic amount of Pd(II) got reduced to metallic Pd.

To better understand the formation process of CPdMs, the intermediate nanocrystals produced at different reaction times were investigated by TEM. As illustrated in Figure 3, as a result of the reductive-oxidative etching cycles caused by the co-presence of CO and Fe^{3+}, the products collected at 25 min were heavily etched at their edges. The average size of the obtained particles was 67 nm. These nanocrystals continued to grow for 60 min. The average size of the particles increased to 142 nm at 30 min, to 168 nm at 45 min, and to 185 nm at 60 min. During the growth of the particles, their branched feature also became more and more prominent with increasing size of each branch. Beyond 1 h, no further change in the size or the morphology of the obtained nanocrystals was observed (Figure S9). These results imply that the etched sites resulting from Fe^{3+} oxidation at the early stage of the reaction served as the growth sites for forming the sheet-like branches.

Thus, the formation of CPdMs reported here undergoes a mechanism of etching growth under surface confinement. CO and Fe^{3+} are two key components in controlling the final morphology of the CPdMs. Fe^{3+} is involved in the oxidative etching process that modifies the laterals of the Pd nanostructures at the early stage and provides active sites for further growth. CO is a decisive factor that confines the growth of the nanosheet branches of CPdMs throughout the growth process. The strong binding of CO on Pd (111) ensures the continuous growth of 2D Pd nanosheets at the etched sites along the original
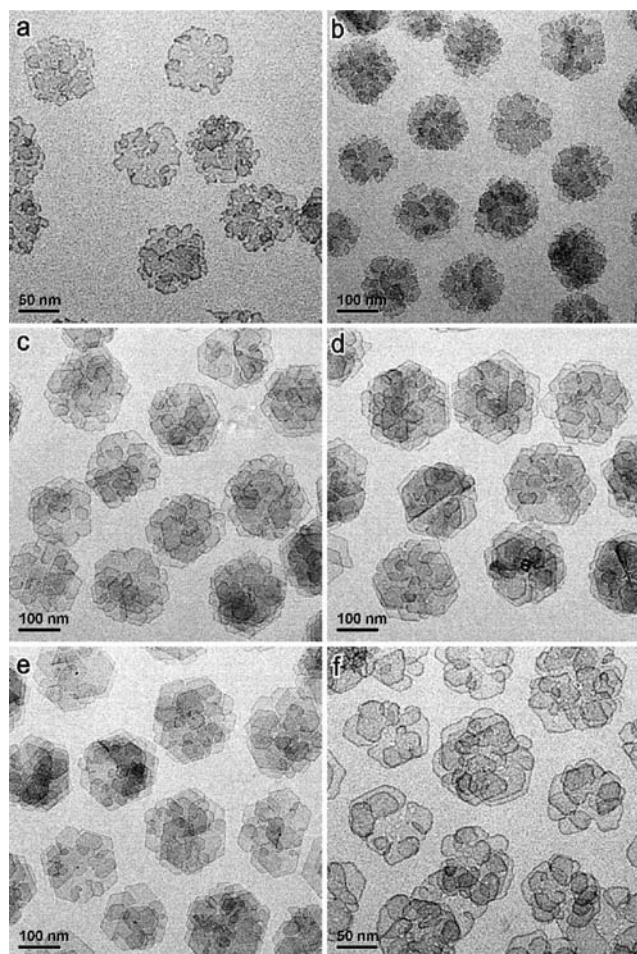
Figure 3. TEM images of CPdMs produced in (a) 25, (b) 30, (c) 45, (d) 60, and (e) 90 min reactions. (f) TEM image of CPdMs obtained under 0.05 mL of $FeCl_3$ (13.5 mg/mL).

Figure 4. (a) Absorption spectra of the as-prepared CPdMs and Pd nanosheets. (b) Photothermal effect of the CPdMs. The temperature vs time plots were recorded from the CPdMs with various concentrations upon irradiation by a 1-W laser. (c) Viability of healthy liver cells incubated for 48 h with different concentrations of the CPdMs. (d,e) Micrographs of cancer cells after 12-h incubation with CPdMs and Pd nanosheets, respectively, and also after 2-min-irradiation by a 2-W, 808-nm laser. The power density is 1.4 W/cm^2. (f) Pd uptake amount of CPdMs and Pd nanosheets as measured by ICP.

growth direction, making it possible to form single-crystalline-like Pd nanocorolla.

On the basis of the above growth mechanism, it is expected that the number of branches of CPdMs should be controllable by the amount of Fe^{3+}. Such an expectation was indeed confirmed experimentally. As shown in Figure 3f, while maintaining the other reaction conditions the same, reducing the Fe^{3+} concentration from 0.50 mM to 0.25 mM decreased the average number of branches/corollas in the Pd mesocrystals from 22 to 10. Together with the reduced number of branches, the size of the CPdMs was also reduced from 185 to 105 nm (Figure S10). The decreased CPdMs size can be explained by the fact that having less etchants (Fe^{3+}) in the reaction produced more nuclei at the early stage. Therefore, to some extent, the mesocrystalline Pd nanocorolla can be manufactured with desired size and number of branches by controlling the reaction duration and the Fe^{3+} concentration.

Two important structural features are associated with the CPdMs: (1) they consist of ultrathin Pd nanosheets, and (2) the Pd nanosheets in each particle are unidirectionally aligned and well spaced but connected to give intraparticle void and increased apparent thickness as compared to individual Pd nanosheets. As a result of the ultrathin nature of the building components, the CPdMs inherit several unique properties of ultrathin Pd nanosheets. First, the EASA of the CPdMs was measured to be
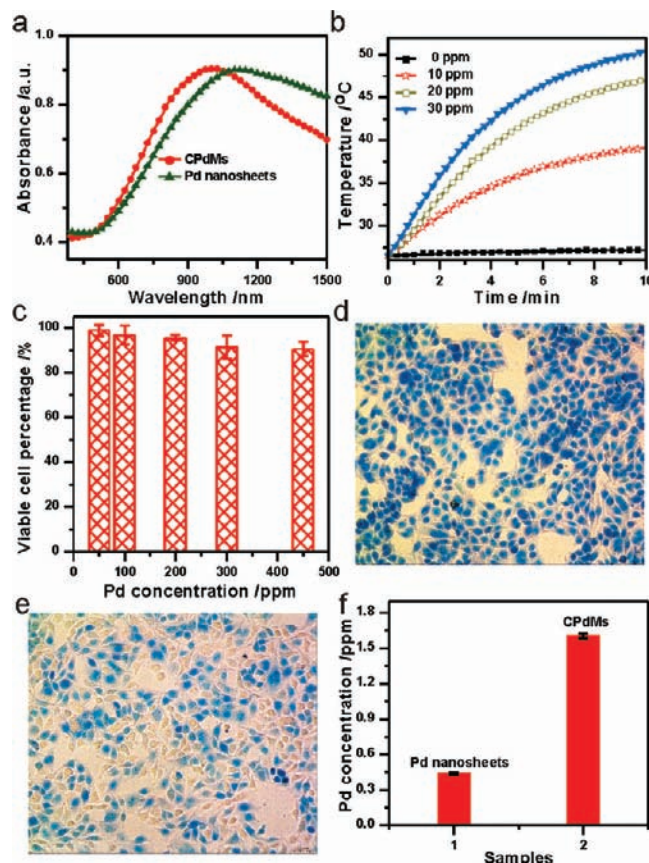
67.2 m^2/g, close to the optimized number obtained on individual Pd nanosheets.[24] Second, similar to individual Pd nanosheets, the CPdMs dispersed in water display a SPR peak in the NIR region (Figure 4a), although the peak is slightly blue-shifted. Resulting from the photothermal effect of CPdMs induced by the NIR SPR absorption, the temperature of a 1-mL solution containing 30 ppm Pd rose from 26.6 to 50.4 °C after 10-min irradiation by an 808-nm laser at 1 W (Figure 4b). Such a photothermal effect is comparable to that of Pd nanosheets.[24] Third, the CPdMs also exhibit excellent biocompatibility. The viable cell count for healthy liver cells was reduced by only 10% after 48-h exposure to a 450 μg/mL solution of the CPdMs (Figure 4c).

Besides inheriting the unique properties of ultrathin Pd nanosheets, the CPdMs also possess properties that do not appear in the single-domain ultrathin Pd nanosheets. For example, the CPdMs are more easily separated by centrifugation than unconnected Pd nanosheets with similar dynamic size ($\sim$190 nm) (Figures S11, S12). Furthermore, when deposited on a flat electrode, the CPdMs created a highly porous architecture to give a specific EASA constant of $\sim$67 m^2/g that does not heavily depend on the amount deposited (Figure S12). In comparison, the specific EASA of Pd nanosheets deposited on a flat electrode can

only be optimized when a small amount of nanosheets is deposited. Due to the possible unfavorable mass tranfer caused by close stacking of the Pd nanosheets, increasing the deposited amout of Pd nanosheets tends to decrease the specific EASA (Figure S13).

As discussed above, the CPdMs display strong NIR SPR absorption and therefore a significant NIR photothermal effect, making them promising for photothermal tumor therapy. After 12-h incubation with CPdMs (20 μg/mL Pd), ~100% of liver cancer cells were killed upon 2-min irradiation with an 808-nm laser (1.4 W/cm^2) (Figure 4d). In comparison, the same irradiation killed only half of the cells incubated with the Pd nanosheets (20 μg/mL Pd) with a similar dynamic size (~190 nm) (Figure 4e). In the absence of Pd nanosheets or CPdMs, the same amount of NIR irradiation did not kill cells (Figure S14). As revealed by our ICP measurements (Figure 4f), the amount of Pd taken up by cells was measured to be 0.44 and 1.60 ppm for Pd nanosheets and CPdMs, respectively. The thicker nature and thus decreased diameter-to-thickness ratio of the mesocrystalline CPdMs allows them to be taken up by cells more easily than the ultrathin Pd nanosheets, consistent with our previous results using silica-coated Pd nanosheets.[32] This result further demonstrates the advantage of mesocrystals over single-domain nanocrystals.

In summary, we have developed an etching growth strategy to prepare corolla-like Pd mesocrystals consisting of ultrathin Pd nanosheets with uniform thickness of 1.8 nm. The co-presence of CO and Fe^{3+} was found critical to the synthesis of the branched CPdMs. The as-prepared Pd mesocrystals not only nicely inherit the unique properties of 1.8-nm-thick Pd nanosheets but also display some outstanding properties that cannot be achieved with single-domain Pd nanosheets, making them promising for electrocatalysis and photothermal therapy applications.

■ ASSOCIATED CONTENT

Ⓢ Supporting Information. Experimental details and additional characterization data. This material is available free of charge via the Internet at http://pubs.acs.org.

■ AUTHOR INFORMATION

Corresponding Author
nfzheng@xmu.edu.cn

■ ACKNOWLEDGMENT

■ REFERENCES

(1) Meldrum, F. C.; Colfen, H. *Chem. Rev.* **2008**, *108*, 4332.
(2) Colfen, H.; Antonietti, M. *Angew. Chem., Int. Ed.* **2005**, *44*, 5576.
(3) Colfen, H.; Mann, S. *Angew. Chem., Int. Ed.* **2003**, *42*, 2350.
(4) Mann, S. *Nat. Mater.* **2009**, *8*, 781.
(5) Wu, X. L.; Xiong, S. J.; Liu, Z.; Chen, J.; Shen, J. C.; Li, T. H.; Wu, P. H.; Chu, P. K. *Nat. Nanotechnol.* **2011**, *6*, 102.
(6) Kulak, A. N.; Iddon, P.; Li, Y. T.; Armes, S. P.; Colfen, H.; Paris, O.; Wilson, R. M.; Meldrum, F. C. *J. Am. Chem. Soc.* **2007**, *129*, 3729.
(7) Pipich, V.; Balz, M.; Wolf, S. E.; Tremel, W.; Schwahn, D. *J. Am. Chem. Soc.* **2008**, *130*, 6879.
(8) Wang, T. X.; Colfen, H.; Antonietti, M. *J. Am. Chem. Soc.* **2005**, *127*, 3246.
(9) Guo, X. H.; Yu, S. H. *Cryst. Growth Des.* **2007**, *7*, 354.
(10) Liu, Z.; Wen, X. D.; Wu, X. L.; Gao, Y. J.; Chen, H. T.; Zhu, J.; Chu, P. K. *J. Am. Chem. Soc.* **2009**, *131*, 9405.
(11) Zhou, L.; Smyth-Boyle, D.; O'Brien, P. *J. Am. Chem. Soc.* **2008**, *130*, 1309.
(12) Ye, J. F.; Liu, W.; Cai, J. G.; Chen, S. A.; Zhao, X. W.; Zhou, H. H.; Qi, L. M. *J. Am. Chem. Soc.* **2011**, *133*, 933.
(13) Hosono, E.; Fujihara, S.; Lmai, H.; Honma, I.; Masaki, I.; Zhou, H. S. *ACS Nano* **2007**, *1*, 273.
(14) Lausser, C.; Colfen, H.; Antonietti, M. *ACS Nano* **2010**, *5*, 107.
(15) Kuang, D. B.; Lei, B. X.; Pan, Y. P.; Yu, X. Y.; Su, C. Y. *J. Phys. Chem. C* **2009**, *113*, 5508.
(16) Tao, J. H.; Pan, H. H.; Zeng, Y. W.; Xu, X. R.; Tang, R. K. *J. Phys. Chem. C* **2007**, *111*, 13410.
(17) Longo, V. M.; Cavalcante, L. S.; Paris, E. C.; Sczancoski, J. C.; Pizani, P. S.; Li, M. S.; Andres, J.; Longo, E.; Varela, J. A. *J. Phys. Chem. C* **2011**, *115*, 5207.
(18) Soejima, T.; Kimizuka, N. *J. Am. Chem. Soc.* **2009**, *131*, 14407.
(19) Fang, J. X.; Du, S. Y.; Lebedkin, S.; Li, Z. Y.; Kruk, R.; Kappes, M.; Hahn, H. *Nano Lett.* **2010**, *10*, 5006.
(20) Huang, X.; Zhang, H.; Guo, C.; Zhou, Z.; Zheng, N. *Angew. Chem., Int. Ed.* **2009**, *48*, 4808.
(21) Xiong, Y. J.; Xia, Y. N. *Adv. Mater.* **2007**, *19*, 3385.
(22) Lim, B.; Xiong, Y. J.; Xia, Y. N. *Angew. Chem., Int. Ed.* **2007**, *46*, 9279.
(23) Huang, X. Q.; Tang, S. H.; Zhang, H. H.; Zhou, Z. Y.; Zheng, N. F. *J. Am. Chem. Soc.* **2009**, *131*, 13916.
(24) Huang, X. Q.; Tang, S. H.; Mu, X. L.; Dai, Y.; Chen, G. X.; Zhou, Z. Y.; Ruan, F. X.; Yang, Z. L.; Zheng, N. F. *Nat. Nanotechnol.* **2011**, *6*, 28.
(25) Xiong, Y. J.; McLellan, J. M.; Chen, J. Y.; Yin, Y. D.; Li, Z. Y.; Xia, Y. N. *J. Am. Chem. Soc.* **2005**, *127*, 17118.
(26) Huang, X. Q.; Zheng, N. F. *J. Am. Chem. Soc.* **2009**, *131*, 4602.
(27) Chen, Y.-H.; Hung, H.-H.; Huang, M. H. *J. Am. Chem. Soc.* **2009**, *131*, 9114.
(28) Jin, R. C.; Cao, Y. C.; Hao, E. C.; Metraux, G. S.; Schatz, G. C.; Mirkin, C. A. *Nature* **2003**, *425*, 487.
(29) Millstone, J. E.; Hurst, S. J.; Metraux, G. S.; Cutler, J. I.; Mirkin, C. A. *Small* **2009**, *5*, 646.
(30) Chen, J. Y.; Herricks, T.; Geissler, M.; Xia, Y. N. *J. Am. Chem. Soc.* **2004**, *126*, 10854.
(31) For the standard potentials of the redox pairs involved in this system:

$$Fe^{3+} + e^- \rightarrow Fe^{2+}, \quad E^0 = 0.771V$$

$$Pd(acac)_2 + 2e^- \rightarrow Pd + 2acac^-, \quad E^0 = 0.149V$$
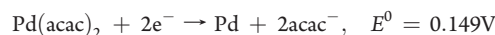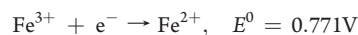
So, Fe^{3+} can oxidize a Pd atom back to Pd(acac)$_2$.
(32) Tang, S. H.; Huang, X. Q.; Zheng, N. F. *Chem. Commun.* **2011**, *47*, 3948.